ELSEVIER

Journal of Alloys and Compounds 223 (1995) 6–12

Journal of ALLOYS AND COMPOUNDS

Amorphous La–Ni thin film electrodes

Yang Li, Yang-Tse Cheng *

Physical Chemistry Department, General Motors R&D Center, Warren, MI 48090-9055, USA

Received 12 September 1994

Abstract

Amorphous La–Ni thin films over a wide range of composition were fabricated by electron beam evaporation in ultra-high vacuum. The structure and composition of these films were determined by X-ray diffraction (XRD), transmission electron microscopy (TEM) and electron probe microanalysis (EPMA). The reversible hydrogen storage capacity was determined by electrochemical cycling. The equilibrium electrochemical potential of these thin-film electrodes was also measured versus the change of hydrogen concentration, ΔH/M, in these films. The smallest value among the maximum ΔH/M of these amorphous films is about 0.38, which is still much larger than the one reported in the literature (~0.1). Harris's model for hydrogen absorption in amorphous transition metal alloys is applied to the amorphous La–Ni system. We found that both the La–Ni_3 and the La_2–Ni_2 type of tetrahedral sites can store hydrogen.

Keywords: Thin film electrodes; Hydrogen storage; Amorphous transition metal alloys

1. Introduction

Many transition metals and their alloys have a high reversible hydrogen absorbing capability [1–5]. They have been used as hydrogen storage and sensing materials [6–8]. Although these metal hydride forming materials have been studied extensively for more than two decades, the structure dependence of the hydrogen absorbing capability is yet to be well understood. While many intermetallic compounds can absorb more hydrogen than their amorphous alloy counterparts, several amorphous transition metal alloys have been found to absorb about the same amount or even more hydrogen than the intermetallic compounds [9,10]. Therefore, hydrogen storage in amorphous materials is of both practical and fundamental interest.

In this study, we further investigated the hydrogen absorbing capability of the amorphous La–Ni system. Amorphous La–Ni thin films over a wide range of compositions were fabricated by electron beam evaporation in ultra-high vacuum (UHV). The reversible hydrogen storage capacity and the equilibrium electrochemical potential of these thin-film electrodes were measured electrochemically. Harris's model for hydrogen absorption in amorphous binary transition metal alloys was applied to the La–Ni system [11]. It is believed that only the La–Ni_3 tetrahedral site is responsible for hydrogen storage in crystalline $LaNi_5$ [12]. We found that both the La–Ni_3 and the La_2–Ni_2 type of tetrahedral sites can store hydrogen in amorphous La–Ni thin films.

2. Experimental

2.1. Thin-film preparation

Thin films were fabricated with the electron-beam evaporation system described previously [13]. Lanthanum (99.9%, Johnson–Matthey) and nickel (99.99%, Johnson–Matthey) were simultaneously deposited onto gold-coated nickel disks, NaCl and quartz substrates to form $LaNi_x$ thin films. The deposition rate of each material was monitored by a Leybold Inficon XTC thickness controller. La–Ni thin films can be fabricated over a wide range of compositions by varying the rates. The pressure during deposition was between 5×10^{-9} and 2×10^{-8} Torr. The electroplated gold coating layer on the Ni disks was about 10 μm thick, sufficient to prevent the detection of the nickel substrate by electron probe microanalysis (EPMA) and X-ray diffraction (XRD). Substrates were cleaned ultrasonically in acetone for about 15 min, then in methanol for another 15 min. They were then transferred into the UHV

* Correspondence should be sent to: Cheng@GMR.com or (Fax) 810-986-8697.

SSDI 0925-8388(94)01500-7

deposition chamber after the pressure inside the load lock decreased below 5×10^{-8} Torr. Substrates were at room temperature (max 45 °C) during deposition.

2.2. Composition and structure determination

The composition and the mass thickness of the films were determined quantitatively by EPMA (25 kV). The thickness was then calculated from the mass thickness and the composition using the assumption that the atomic volume of the film is the weighted average of the atomic volume of the bulk lanthanum and nickel. Films deposited on Au-coated Ni disks were examined by XRD in Seemann–Bohlin and θ–2θ geometry, both with Cu Kα radiation. For transmission electron microscopy (TEM) samples were deposited onto NaCl substrates and the substrates were then dissolved in distilled water. A Surface Science Instruments SSX-100 X-ray photoelectron spectroscope (XPS) with a sputter ion gun (4 kV, Ar^+) was used to measure the depth profile and to determine the C and O impurity levels in the films.

2.3. Electrochemical cycling

The experimental set-up described in a previous report [13] was used for electrochemical cycling. Films deposited on the quartz substrates were used in electrochemical cycling and equilibrium electrochemical potential measurements. The contact area between the working electrode and the electrolyte (6 M KOH) was about 0.34 cm^2 and the charge–discharge current was ∓0.05 mA. These electrodes were charged until hydrogen evolution occurred on the electrode surface. The discharge period was terminated when the potential increased to -0.5 V vs. Hg/HgO. The discharge capacity was calculated as the product of the discharge time and the current.

The equilibrium potential vs. the reversible hydrogen concentration (ΔH/M) curves of the La–Ni films were measured at room temperature (25 ± 1 °C). After a short period (<1 min) of charging, the potential of the La–Ni electrode vs. Hg/HgO became stable and was recorded as the equilibrium potential. A known amount of charge was then discharged from the working electrode at a 0.05 mA rate and the new equilibrium potential was recorded when the potential did not change vs. time. This procedure was continued until the potential reached -0.5 V vs. Hg/HgO during discharge.

3. Results and discussion

3.1. Structure and composition

The TEM electron diffraction patterns and plan-view images of $LaNi_3$ and $LaNi_5$ films deposited at room temperature are shown in Fig. 1. Evidently, neither electron diffraction spots nor sharp rings is observed. Films on Au-coated Ni substrates were examined by Seemann–Bohlin XRD and thicker films were subjected to θ–2θ XRD. No diffraction peaks were found in either case. Therefore, films of all compositions deposited at room temperature are said to be amorphous.

The distinct character of amorphous metallic alloys is the lack of long-range atomic order, in contrast to the crystalline compounds [14,15]. Several quenching methods, such as melt-spinning, rapid splat-quenching and condensation from the gas phase (see Fig. 2), can be used to produce amorphous metallic alloys [16]. The key factor is the cooling rate. At high cooling rates, atoms quickly lose their kinetic energy and become immobilized. Hence, they do not have enough time to find the lowest-energy site and can only form a thermodynamically metastable structure [16]. Melt-spinning, rapid splat-quenching and vapor condensation techniques have the cooling rate about 10^6, 10^5–10^8 and 10^{10}–10^{12} K s^{-1}, respectively [16]. Obviously, the vapor condensation technique has the largest cooling rate, which enhances the probability of forming amorphous alloys. It is generally accepted that the amorphous alloy film is more likely to form when the temperature of the substrate during deposition is low [17]. Moreover, the different crystal structures of lanthanum (h.c.p.) and nickel (f.c.c.), a negative heat of formation [18] and a large difference in atomic sizes of lanthanum and nickel facilitate amorphous-phase formation by co-deposition [14]. Furthermore, amorphous La–Ni thin films at the $LaNi_5$ intermetallic compound composition can also be fabricated by electron-beam evaporation [13] and by radio-frequency (RF) sputtering [19,20].

The composition and mass thickness of the set of $LaNi_x$ ($1<x<5$) thin films determined by EPMA is given in Table 1, along with the calculated thickness (about 500 Å). The results from XPS depth profiling show that these films are uniform and impurity levels of C and O are below the detection limit of this XPS system (2 at.%).

This study is the first to show that amorphous $LaNi_x$ ($1<x<5$) can form over a wide composition range.

3.2. Electrochemical measurement

The amorphous $LaNi_x$ ($1\leqslant x\leqslant5.5$) thin films were first cycled electrochemically for about 10 cycles for activation. A typical potential (vs. Hg/HgO) versus charge–discharge time curve of an amorphous La–Ni is presented in Fig. 3. Evidently, no plateau exists which is consistent with other reported studies on amorphous metal hydrogen systems [19,21–23]. The measurement of the equilibrium electrochemical potential vs. the reversible hydrogen concentration was conducted when the films reached their maximum discharge capacity. The reversible hydrogen concentrations, ΔH/M, deter-

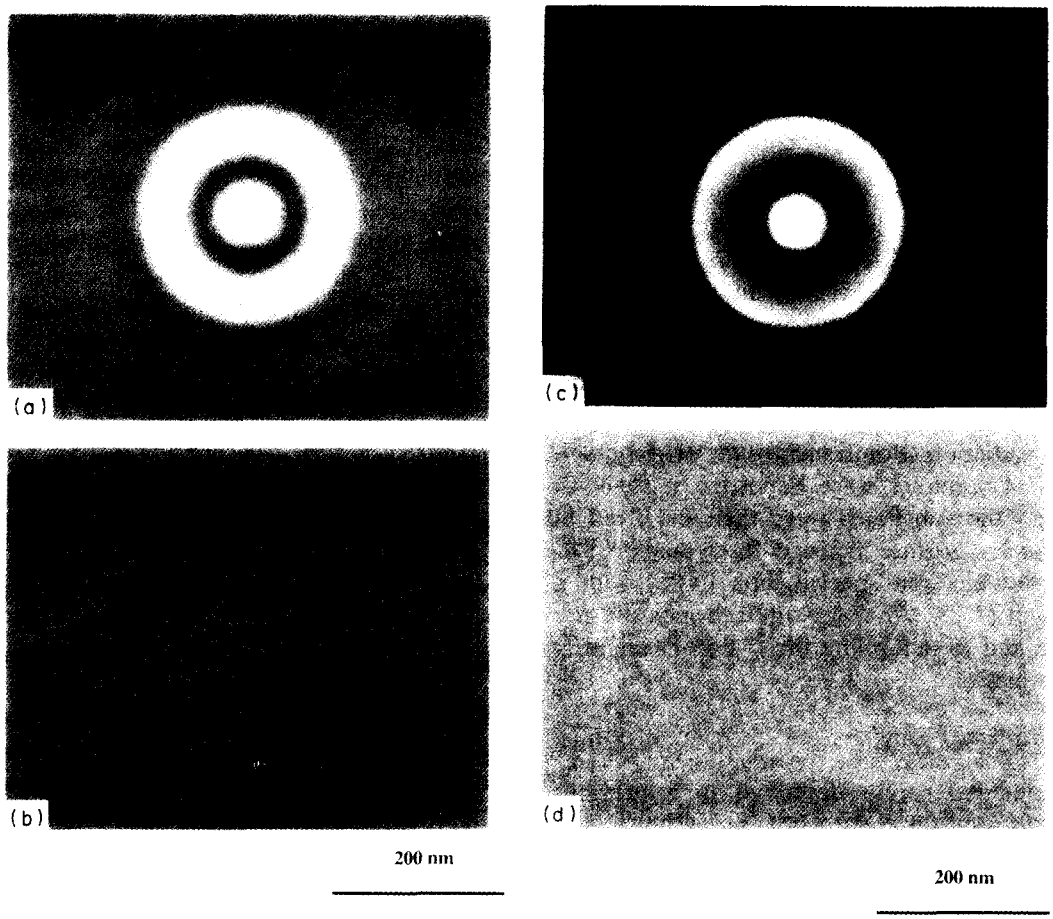

Fig. 1. Amorphous $LaNi_3$ thin film: (a) electron diffraction pattern and (b) corresponding plan-view image. Amorphous $LaNi_5$ thin film: (c) electron diffraction pattern and (d) corresponding plan-view image.

mined from this measurement are also given in Table 1. These amorphous thin films have at least three times or more the discharge capacity of the ones fabricated by RF sputtering that were reported in the literature [20].

3.3. Model of hydrogen site in amorphous transition metal alloys

Harris et al. have presented a comprehensive hydrogen-site statistical model for the total and electrochemically reversible hydrogen storage in binary amorphous transition metal alloys $A_{1-x}B_x$ (where A (B) is a late (early) transition metal) [11]. The alloy is considered structurally isomorphic and chemically random. Hydrogen atoms are stored in tetrahedral interstitial sites $A_{4-n}B_n$, where $n=1$ to 4 [11]. The probability $f_n(x)$ of four neighboring atoms in $A_{1-x}B_x$ being an $A_{4-n}B_n$ site is proportional to $C_4^n x^n (1-x)^{4-n}$, where $C_4^n = 4!/n!(4-n)!$. The energy of each type of site (n) is a continuous distribution $g_n(E)$. Therefore, the density of states (DOS) of each site is proportional to $f_n(x) \cdot g_n(E)$ and the change of hydrogen concentration $\Delta H/M$ due to this particular site n is

$$\Delta H/M = N_{\text{eff}} \cdot f_n(x) \cdot \int_{-\infty}^{+\infty} g_n(E)\, dE \quad (1)$$

where N_{eff} is a proportionality factor [11]. Harris et al. determined the chemical potential μ of the absorbed hydrogen in the transition metal electrode by measuring the equilibrium potential difference between the transition metal electrode and the reversible hydrogen electrode at different hydrogen concentrations. They demonstrated that a universal curve can be used to fit μ (from -100 to -38.5 kJ mol^{-1} of H_2) versus normalized changes of hydrogen concentration $(\Delta H/M|_{\text{exp}})/(\Delta H/M|_{\text{max}})$ for amorphous $Ni_{1-x}Zr_x$ over the composition $x=0.37$ to 0.70 (see Fig. 4), where -100 kJ mol^{-1} of H_2 is the μ_{min} due to their experimental limitation and -38.5 kJ mol^{-1} of H_2 is the μ_{max} at hydrogen evolution [11]. This universal curve was constructed using a normalized Gaussian distribution function,

$$g(E) = \frac{1}{\sigma\sqrt{\pi}} \exp\left[-\left(\frac{E-E_0}{\sigma} \right)^2 \right] \quad (2)$$

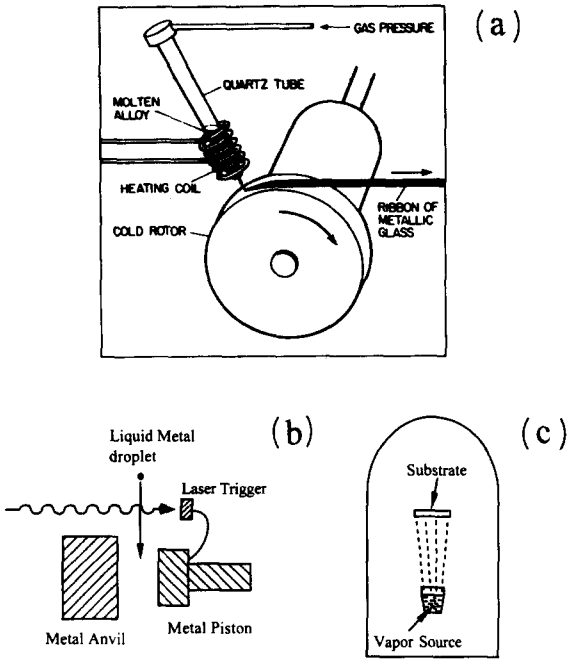

Fig. 2. Schematic representation of several methods of forming amorphous solids: (a) melt-spinning; (b) rapid splat-quenching; (c) vapor condensation.

to approximate the $g_2(E)$ between μ_{min} and μ_{max}. Furthermore, they determined N_{eff} to be 1.9 from two amorphous Ni–Zr and Pd–Ti systems, assuming that only the Ni_2Zr_2 and $PdTi_3$ tetrahedral sites are responsible for reversible hydrogen storage in $Ni_{1-x}Zr_x$ and $Pd_{1-x}Ti_x$, respectively [11]. A schematic representation of the density of states versus the chemical potential μ is shown in Fig. 5. The center E_0 and width σ or the Gaussian distribution was -58.5 and 25.0 kJ mol^{-1} of H_2, respectively, determined from their experimental data. Hence, for the Ni–Zr system, Eq. (1) becomes

$$\Delta H/M|_{exp} = 1.9C_4^2 \cdot x^2(1-x)^2 \int_{\mu min}^{\mu max} g_2(E)\, dE \quad (3)$$

Thus, the change of hydrogen concentration versus film composition should follow the $x^2(1-x)^2$ binomial function. Harris et al. demonstrated experimentally that Eq. (3) was indeed valid [11]. The total hydrogen concentration at a certain chemical potential μ is the summation of all the possible sites that lie below μ. In the case of Ni–Zr,

$$H/M(\mu) = 1.9[x^4 + 4x^3(1-x) + 6x^2(1-x)^2 \int_{\mu min}^{\mu} g(E)\, dE] \quad (4)$$

since the integrals of $g_4(E)$ and $g_3(E)$ from $-\infty$ to μ_{min} are approximately 1.

The center E_n of the distribution of each site was considered as the enthalpy of formation of the hydride, which was estimated based on the Rudman and Sandrock "rule of simple averaging" model [24],

$$E_n = [nH_0(BH_2) + (4-n)H_0(AH)]/4 \quad (5)$$

Here H_0 is denoted as the enthalpy of formation of elemental hydrides such as BH_2 and AH. This model differs from the "rule of reversed stability" proposed by Buschow et al. [25],

$$\Delta H(AB_nH_{2m}) = \Delta H(AH_m) + \Delta H(B_nH_m) - \Delta H(AB_n) \quad (6)$$

by the enthalpy of formation of the alloy term, $\Delta H(AB_n)$. Since the effect of H-atom insertion on AB bonding strengths is not well understood, the rule of simple averaging is considered as good as the rule of reversed stability, especially for the purpose of estimating the distance of two adjacent distribution centers [24].

The separation between adjacent E_n is about 44 kJ mol^{-1} of H_2 for the Ni–Zr system, which is almost twice the value of σ. Therefore, it is justifiable to make the assumption that only Ni_2Zr_2 is the hydrogen storage site within the μ_{min} and μ_{max} experimental window.

The equilibrium electrochemical potentials E of the amorphous $Ni_{1-x}La_x$ thin films were converted to chemical potential μ (expressed as kJ (mol H_2)$^{-1}$) by

$$\mu = -2F(0.932 + E) \quad (7)$$

where F is the Faraday constant and 0.932 is the potential difference between Hg/HgO and the reversible hydrogen

Table 1
Hydride formation versus composition for a set of amorphous $LaNi_x$ thin films

Amorphous alloy	La (at.%)	Ni (at.%)	Mass thickness ($\mu g\ cm^{-2}$)	Thickness (Å)	Maximum discharge capacity (mA h g^{-1})	ΔH/M
LaNi	50.3	49.7	33.3	490	108	0.40
$LaNi_{1.7}$	37.0	63.0	32.8	460	144	0.48
$LaNi_{2.8}$	26.5	73.5	35.7	480	126	0.38
$LaNi_{3.5}$	22.0	78.0	35.2	460	174	0.50
$LaNi_{4.8}$	17.2	82.8	38.5	490	170	0.46

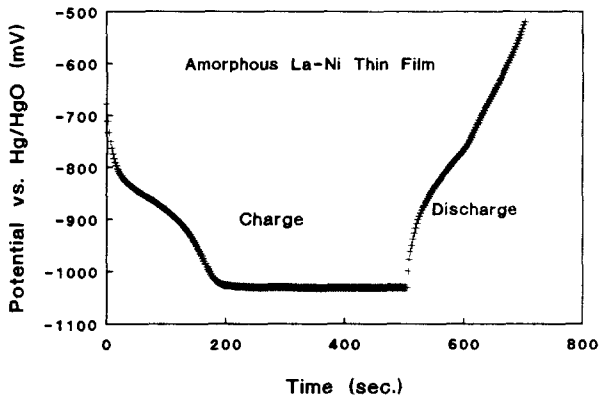

Fig. 3. A typical electrode potential (vs. Hg/HgO) vs. charge–discharge time curve of amorphous La–Ni thin films.

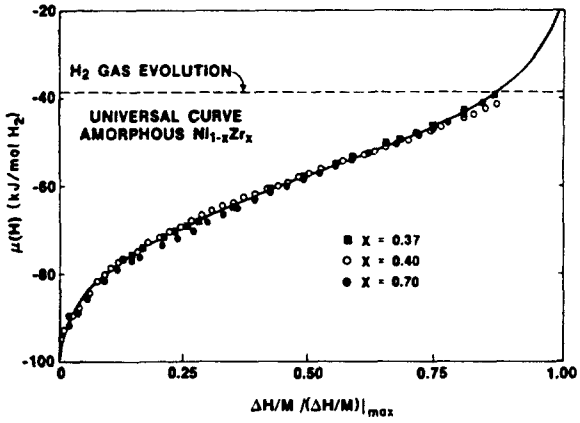

Fig. 4. Chemical potential μ of hydrogen in $Ni_{1-x}Zr_x$ vs. total normalized hydrogen concentration $(\Delta H/M|_{exp})/(\Delta H/M|_{max})$ at different compositions ($x=0.37$, 0.40, and 0.70) [11].

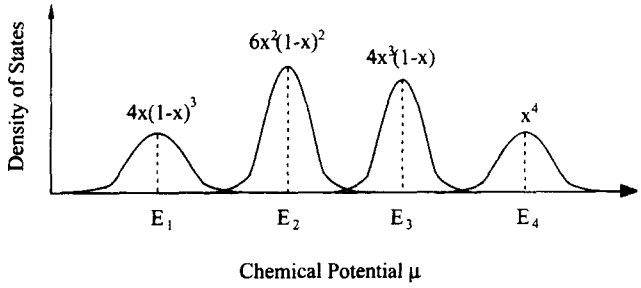

Fig. 5. Density of states $f_n(x)\cdot g(E)$ vs. chemical potential μ of hydrogen in various tetrahedral interstitial sites.

electrode (RHE) [25]. The chemical potential of the absorbed hydrogen versus ΔH/M was then calculated for all the films. It has been demonstrated that La–Ni_3 is the primary hydrogen storage site in crystalline $LaNi_5$ [12]. Assuming that this tetrahedral site is the only hydrogen storage site in the La–Ni system, the change of hydrogen concentration vs. μ based on Harris's model should be

$$\Delta H/M(\mu) = 1.9[4x^3(1-x)\int_{\mu_{min}}^{\mu} g_1(E)\,dE] \quad (8)$$

However, we have difficulty in fitting the μ vs. ΔH/M curves for all the compositions.

Assuming that the La_2–Ni_2 tetrahedral site can also store some hydrogen, two Gaussian distribution functions are used to fit the ΔH/M vs. μ curves for all compositions (see Fig. 6). The center of the distribution function for the La–Ni_3 site, E_1, is estimated to be -43 ± 1 kJ (mol H_2)$^{-1}$ with a width σ_1 of 16 ± 1 kJ (mol H_2)$^{-1}$ while E_2 (for the La_2–Ni_2 site) is -84 ± 1 kJ (mol H_2)$^{-1}$ with a width σ_2 of 15 ± 1 kJ (mol H_2)$^{-1}$ in order to have the best fit for the ΔH/M vs. μ curves for different compositions. These ΔH/M vs. μ curves are shown in Fig. 7. The enthalpies of formation of La–H and Ni–H bonds are given in Table 2 [24,27], along with E_1 and E_2, obtained from both fitting the ΔH/M vs. μ curves and calculation based on Eq. (5). Comparing the results listed in Table 2, E_1 and E_2 obtained from curve fitting are not unreasonable. The solid line is obtained by

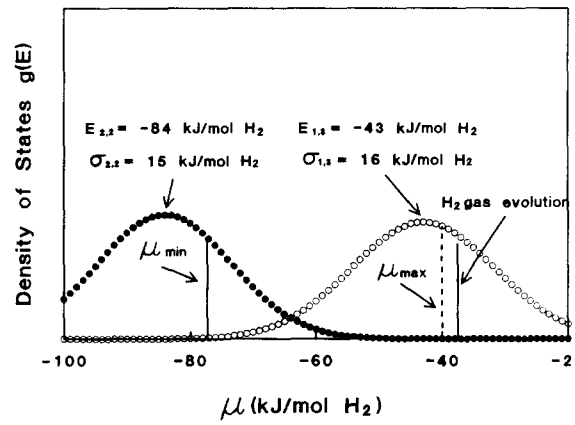

Fig. 6. Normalized density of states $g(E)$ for $LaNi_3$ and La_2Ni_2 tetrahedral sites vs. chemical potential μ of hydrogen.

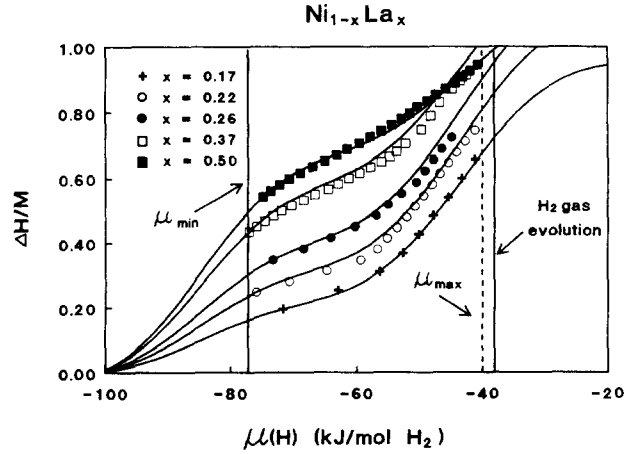

Fig. 7. Change of hydrogen concentration ΔH/M vs. chemical potential μ of hydrogen in amorphous La–Ni thin films.

Table 2
Enthalpy of formation ((kJ (mol H_2)$^{-1}$) of ternary hydride based upon "rule of simple averaging" and E_1, E_2 obtained from curve fitting

LaH_2	NiH	E_1 ($LaNi_3$ site)	E_2 (La_2Ni_2 site)
−207.75 [24]	16.62 [24]	−39.5	−95.6
−134 [26]	−2 [26]	−35	−68
		−43 (curve fitting)	−84 (curve fitting)

$$\Delta H/M(\mu) = 1.9[4x^3(1-x)\int_{\mu_{min}}^{\mu} g_1(E)\,dE + 6x^2(1-x)^2\int_{\mu_{min}}^{\mu} g_2(E)\,dE] \quad (9)$$

where $g_1(E)$ and $g_2(E)$ are the normalized Gaussian distribution functions for the La–Ni_3 site and La_2–Ni_2 site, respectively, and $\mu_{min} = -100$ kJ (mol H_2)$^{-1}$. The $\Delta H/M$ value at the lowest μ value of each film was determined by Eq. (9), and the rest of the points were from the potential composition isotherm measurements. The lower and upper limits (μ_{min} and μ_{max}) in this experiment are about −77 and −40 kJ (mol H_2)$^{-1}$, respectively. Evidently, the chemical potential of several films did not reach either μ_{min} or μ_{max}, or both. These films were not charged to their full hydrogen storage capacity. Some of the hydrogen atoms are evolved as gas instead of being absorbed by the film during the charging period. Fig. 7 suggests that this model can be used to predict the hydrogen concentration in La–Ni amorphous alloys. Moreover, it also suggests that if the width (2σ) of the DOS (Gaussian distribution) lies within the electrochemical potential window, from the oxidation potential to the hydrogen evolution potential, amorphous material could store as much hydrogen as the crystalline counterpart. Furthermore, it is possible for amorphous alloys with overlapping DOS distributions within the electrochemical potential window to store more hydrogen than the crystalline compounds. This model can provide a new guideline in the search for novel metal hydride materials.

4. Conclusions

Amorphous $LaNi_x$ ($1 \leqslant x \leqslant 5.5$) thin films have been prepared by electron-beam evaporation in UHV. Their composition and structure were determined by EPMA, XRD and TEM. Electrochemical experiments showed that (a) the amorphous $LaNi_x$ ($3 \leqslant x \leqslant 5$) thin films have a maximum reversible hydrogen storage capacity of about 160 mA h g^{-1} (H/M ~ 0.43) and cycle life of about 500 cycles; (b) both the La–Ni_3 and La_2–Ni_2 tetrahedral sites contribute to hydrogen storage and Harris's model can be used to predict hydrogen storage capacity.

Acknowledgments

We would like to thank R. Waldo for EPMA, J. Chen for TEM, and W.J. Meng, F.T. Wagner, D.N. Belton, M.A. Habib, C.L. Dimaggio, T.E. Moylan and S.J. Schmieg for helpful discussions. This work is supported by General Motors Corporation.

References

[1] J.J. Reilly and R.H. Wiswall Jr., *Inorg. Chem., 7* (1968) 2254.
[2] J.J. Reilly and R.H. Wiswall Jr., *Inorg. Chem., 11* (1974) 218.
[3] K. Suzuki, *J. Less-Common Met., 89* (1983) 183.
[4] D.A. Smith, I.P. Jones and I.R. Harris, *J. Less-Common Met., 103* (1984) 33.
[5] J.H.N. Van Vucht, F.A. Kuijpers and H.C.A.M. Bruning, *Philips Res. Rep., 25* (1970) 133.
[6] Y.T. Cheng, Y. Li, D. Lisi and W.M. Wang, *Sensors and Actuators B,* accepted for publication.
[7] R.C. Hughes and W.K. Schubert, *J. Appl. Phys., 71*(1) (1992) 542.
[8] P.F. Ruths, S. Ashok, S.J. Fonash and J.M. Ruths, *IEEE Trans. Electron Devices, ED28* (1981) 1003.
[9] Y. Sakamoto, T.B. Flanagan and T. Kuji, *Z. Phys. Chem., 143* (1985) 61.
[10] A.J. Mealand, L.E. Tanner and G.G. Libowitz, *J. Less-Common Met., 74* (1980) 279.
[11] J.H. Harris, W.A. Curtin and M.A. Tenhover, *Phys. Rev. B, 36* (1987) 5784.
[12] C.E. Lundin, F.E. Lynch and C.B. Magee, *J. Less-Common Met., 56* (1977) 19.
[13] Y. Li, Y.-T. Cheng and M.A. Habib, *J. Alloys Comp., 209* (1994) 7.
[14] Y.-T. Cheng and W.L. Johnson, *Science, 235* (1987) 997.
[15] K.H.J. Buschow, in K.A. Gschneidner Jr. and L. Eyring (eds.), *Handbook on the Physics and Chemistry of Rare Earths,* North-Holland, New York, 1984.
[16] R. Zallen, in *The Physics of Amorphous Solids,* John Wiley & Sons, New York, 1983.
[17] P. Chaudhari and D. Turnbull, *Science, 199* (1979) 11.

[18] W.L. Johnson, *Prog. Mater. Sci., 30* (1986) 81.
[19] G. Adachi, K.I. Niki, H. Nagai and J. Shimokawa, *J. Less-Common Met., 88* (1988) 213.
[20] T. Sakai, H. Ishikawa, H. Miyamura, N. Kuriyama, S. Yamada and T. Iwasaki, *J. Electrochem. Soc., 138* (1991) 908.
[21] F.H.M. Spit, J.W. Drijver, W.C. Turkenurg and S. Radelaar, *Scr. Metall., 14* (1980) 1071.
[22] R. Kirchheim, F. Sommer and G. Schluckebier, *Acta Metall., 30* (1982) 1059.
[23] G.G. Libowitz and A.J. Mealand, *J. Less-Common Met., 101* (1984) 131.
[24] P.S. Rudman and G.D. Sandrock, *Annu. Rev. Mater. Sci., 12* (1982) 271.
[25] K.H.J. Buschow, P.C.P. Bouten and A.R. Miedema, *Rep. Prog. Phys., 45* (1982) 937.
[26] J.J.G. Willems, *Philips J. Res., 39* (1984).
[27] P.C.P. Bouten and A.R. Miedema, *J. Less-Common Met., 71* (1980) 147.